Carbon additive effect on the electrochemical performances of inkjet printed thin-film $Li_4Ti_5O_{12}$ electrodes

Prisca Viviani [a,1], Eugenio Gibertini [a,1], Filippo Iervolino [b], Marinella Levi [b], Luca Magagnin [a,*]

[a] *Dipartimento di Chimica, Materiali e Ingegneria Chimica "Giulio Natta", Politecnico di Milano, Via Luigi Mancinelli 7, 20131 Milan, Italy*
[b] *Dipartimento di Chimica, Materiali e Ingegneria Chimica "Giulio Natta", Politecnico di Milano, Piazza Leonardo da Vinci 32, 20133 Milan, Italy*

Keywords Anode, Li-ion battery Inkjet printing Carbon nanotube Ink formulation

1. Abstract

Conventional rigid batteries find limited applications in the wearable and flexible electronics field, as difficulties in device integration due to lack of shape conformability to unconventional substrates remain an obstacle. Accordingly, new fabrication techniques are under investigations and printing techniques have attracted great interest for their selectivity, low material waste and scalability. In this frame, inkjet printing (IJP) has emerged as a potential fabrication technique to obtain flexible patterned thin-film electrodes with high resolution. However, a more in-depth systematic study of how IJP can be applied to lithium-ion batteries fabrication is still missing. Herein, we propose a study that focuses on how different carbon-based additives (Nitta et al., 2015; Choi and Ahn, 2018 [1,2]), i.e. carbon black and multi-walled carbon nanotubes, affect the electrochemical performances of inkjet printed thin-films $Li_4Ti_5O_{12}$ electrodes. A simple ink formulation is proposed, which is aqueous-based, non-toxic and safe to handle. The fabricated thin-film electrodes showed different specific capacity, the highest associated with the carbon nanotubes-based (CNTs) electrode, i.e. 150.3 mAh g^{-1} at 0.2 C, showing that CNTs improving electrochemical performances can be applied also to printed electrodes. The carbon nanotubes-based electrodes showed excellent cycle stability, with negligible capacity loss for over 100 cycles. The work highlights the importance of a valid material choice to reach the desired electrode performances and may inspire alternatives paths to deepen IJP of lithium-ion batteries fabrication.

2. Introduction

Lithium-ion batteries (LIBs) represent the to-go energy storage technology in many application fields as portable electronics, power instruments and automotive due to their unique combination of high energy and power density [1]. However, the use of rigid and traditional batteries, as well as their respective fabrication processes, is limited when dealing with wearable electronics [2]. In particular, when patterned electrodes, thin films and unconventional substrates are involved, new fabrication strategies are needed in order to overcome the limitations of the traditional slurry coating roll-to-roll electrode processing [3]. Conventional thin film fabrication techniques, as Chemical Vapor Deposition (CVD) [4], Atomic layer deposition (ALD) [5] or magnetron sputtering [6] are able to produce thin electrodes with extremely accurate thickness and composition control but they require controlled environments, complex processes and high costs [7]. As a consequence, academic and industrial interest was driven towards alternatives and printing techniques are a class of technologies particularly interesting for their low cost, versatility and scalability [8–12]. Inkjet printing (IJP) is one of the most mature and widely used printing technologies and micro-fabrication by IJP has already been demonstrated in many fields [13–18]. IJP is a solution-based mask-less additive technique that can deposit layers of different materials by propelling droplets of ink onto various substrates, allowing minimum material waste and high precision. In addition, the possibility of finely tuning the film thickness, the ambient operative condition and versatility on pattern variation reveal the broad spectrum of opportunities that this technique is able to offer [19]. In Drop-on-Demand inkjet system (DOD) droplets are expelled only when they are needed. Traditional DOD systems work through either a thermal or piezoelectric system [20]. In thermal IJP, small bubbles are created inside the ink chamber when resistors are sufficiently heated upon a voltage application, increasing the pressure inside the chamber and forcing ink droplets through the nozzle [21,22]. This poses some limitations in ink printability, since the

solvent should have a sufficiently low boiling point (i.e. <200 °C) [23]. For this reason, aqueous inks are preferable when dealing with thermal IJP. Furthermore, inks should meet specific physical properties in terms of viscosity (i.e. 2–30 cP) and surface tension (i.e. up to 60 mN m^{-1}), in order to guarantee ink printability [24].

Despite its suitability for high-accuracy patterning and thin-film deposition, to date poor attention has been addressed to the use of IJP for Li-ion micro-battery fabrication. Only few reports exist in literature on IJP printed electrodes, focused on ink formulation for specific active materials as SnO_2 [25], sulfur [26], SiO_2 [19], $Li_4Ti_5O_{12}$ [27], $LiCoO_2$ [28], $LiFePO_4$ [29,30] and MnO_2 [31]. Other works, then, focused on printable electrolyte [32], binder choice [33] and carbon-black surface functionalization affecting ink stability and printability [34]. It is widely known that a good active material electrification is fundamental in order to fully extract the electrode capacity. Generally, carbon-based materials are the easiest available and most employed conductive agents. Of course, different carbon forms have different crystallinity, morphology, particles sizes, and these differences affect the overall conductivity and, eventually, the electrochemical performances [35,36]. In Li-ion battery electrode processing, carbon black (CB) nanoparticles are typically used but graphenic powders and carbon nanotubes (CNT) have been proposed as alternatives [37–40]. Regarding the formulation of IJP inks in literature, carbon-black nanoparticles are commonly used as conductive additive and only PEDOT:PSS was proposed as an electrically conductive binder for SiO_2 nanoparticles-based ink [19]. However, despite different carbon additive effect on electrochemical performances has been previously investigated, those works are related to conventional slurry coating technique and not to inkjet printing. A systematic investigation of conductive additive effect in inkjet printable inks is missing in literature. To fill this lack, we formulated aqueous inks processing $Li_4Ti_5O_{12}$ (LTO) particles with carbon black (CB) and multi-walled carbon nanotubes (MWCNTs) as conductive additives. Table S1 collects different ink formulations present in literature, in order to compare them with the ones presented in this work. The inks were then inkjet printed on a copper foil to obtain thin-film electrodes. We propose a clear comparison in terms of inks rheological properties, in-plane electrical conductivity, electrodes morphology, specific capacity and rate capability according to the carbon conductive additive. Herein, we demonstrate that significantly better electrochemical performances by using MWCNTs instead of CB can be achieved for electrodes obtained through IJP.

3. Experimental

3.1. Ink preparation

In a typical procedure, 1.5 g of $Li_4Ti_5O_{12}$ powder (Tob New Energy Technology Co.), 0.21 g of polyvynilpirrolidone (PVP 40 k, TCI) and 0.187 g of carbon-based conductive agent, either CB (VULCAN XC72, Cabot, 240 m^2 g^{-1}) or CNT (MWCNT, Nanografi, 510 m^2 g^{-1}), were ball-milled at 420 rpm for 8 h with 2.5 ml of ethylene glycol (EG) and 2.5 ml 2-propanol (IPA). A second ball-milling step was done for 1 h at 150 rpm after adding 40 ml aqueous solution of 1 mM lithium dodecyl sulfate (LDS, Sigma-Aldrich) and 0.4 g of lithium polyacrylate (Li-PAA), according to [41]. The stable suspension was then ultrasonically dispersed for 15 min (300 W, 1 s ON, 2 s OFF). The obtained suspension was ready to be used as ink, named LTO-no add, when no conductive agent has been added, LTO-CB when the added conducting agent was CB and LTO-CNT when the added conducting agent was CNTs.

3.2. Preparation of thin-film electrodes

LTO inks were transferred to a properly cleaned HP45 cartridge and then inkjet printed through a flat-bed Breva thermal inkjet printer on a Cu substrate previously coated with a graphite spray. The cartridge had an integrated printhead featuring 300 nozzles with a diameter of ~30 µm, providing a resolution of 600 dpi. Printer parameters values to fire a single drop from nozzles were set to 11.5 V as pulse voltage and 2.2 µs as pulse duration. The printing process was repeated for ten times. The as-printed LTO electrodes were then dried in an oven at 80 °C in vacuum for 3 h prior to the electrochemical characterization.

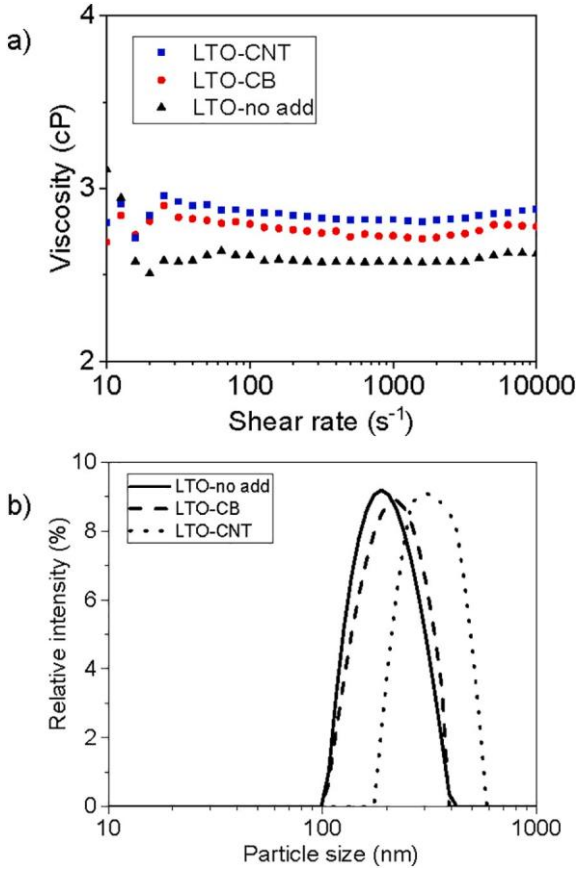

Fig. 1. Viscosity vs shear rate of LTO-CNT (blue), LTO-CB (red) and LTO-no add (black) (a), particle size distribution profile of LTO-no add (solid), LTO-CB (dashed) and LTO-CNT (dotted) inks.

3.3. Characterization

3.3.1. Ink characterization

Rheological properties were measured by means of an Antoon Paar rheometer (MCR-302) with a plane-plane geometry, with a gap of 0.2 mm and a material volume of 110 µl. A samples pre-shearing (at 1000 s^{-1} for 45 s) was performed to assure that all samples have the same mechanical history. Viscosity was measured as function of the shear rate from 0.1 to 10,000 s^{-1}. Data are shown starting from 10 s^{-1}. Surface tension measurement was performed by pendant drop technique and drop shape analysis fitted through Opendrop software. Zeta potential and particle size distribution analysis were performed by means of a Zetasizer (Malverne Instruments).

3.3.2. Printed electrode characterization

Electrode morphology and composition was investigated through Scanning electron microscopy (SEM, Zeiss EVO 50 EP) and energy dispersive spectroscopy (EDS, Oxford instruments INCA x-sight detector). Samples resistivity was characterized by mean of a Keithley 2612B System SourceMeter coupled with the SPP4 S/F Multi Contact four-point needle probes. The tested samples had a length of 80 mm, a width of 50 mm and a thickness of about 1.5 µm. The tests were performed varying

Table 1
Viscosity, surface tension, density, Oh^{-1}, zeta potential and particles size values for LTO-no add, LTO-CB and LTO-CNT inks.

	Viscosity (cP)	Surface tension (mN m^{-1})	Density (kg m^{-3})	Oh^{-1}	Z (mV)	Particle size (nm)
LTO-no add	2.58	40.3	1030	13.47	−34.6	~200
LTO-CB	2.71	40.94	1040	12.92	−38.4	~250
LTO-CNT	2.82	40.41	1040	12.79	−39.6	~330

the current and registering the corresponding voltage. The resistance values were obtained computing the slope of the voltage-current diagram according to Ohm's first law. Resistivity values were obtained accordingly to Ohm's second law, knowing the geometry of the samples. The inkjet printed electrodes were tested by assembling coin cells (CR2032) with Li foil as counter and reference electrode, Celgard 2400 as separator and 50 µl of 1 M $LiPF_6$ in EC:DEC (1:1 vol.) as electrolyte. The cells were assembled in a glove box (MBraun) filled with argon gas (H_2O, O_2 < 0.5 ppm). Cyclic voltammetries (CV) curves were performed through Biologic (VMP3 potentiostat) in a voltage window of 1–3 V vs Li^+/Li at different scan rates. Galvanostatic charge-discharge curves were obtained with Neware cycle tester, in the same voltage window by varying the C-rate, i.e. 0.2, 0.5 and 1C. EIS measurements were performed with Biologic in the frequency range 5 MHz – 0.1 Hz and 10 mV pulse amplitude. All measurements were performed at room temperature.

4. Results & discussion

4.1. Ink rheology and characterization

LTO-no add, LTO-CB and LTO-CNT inks characterization was per-

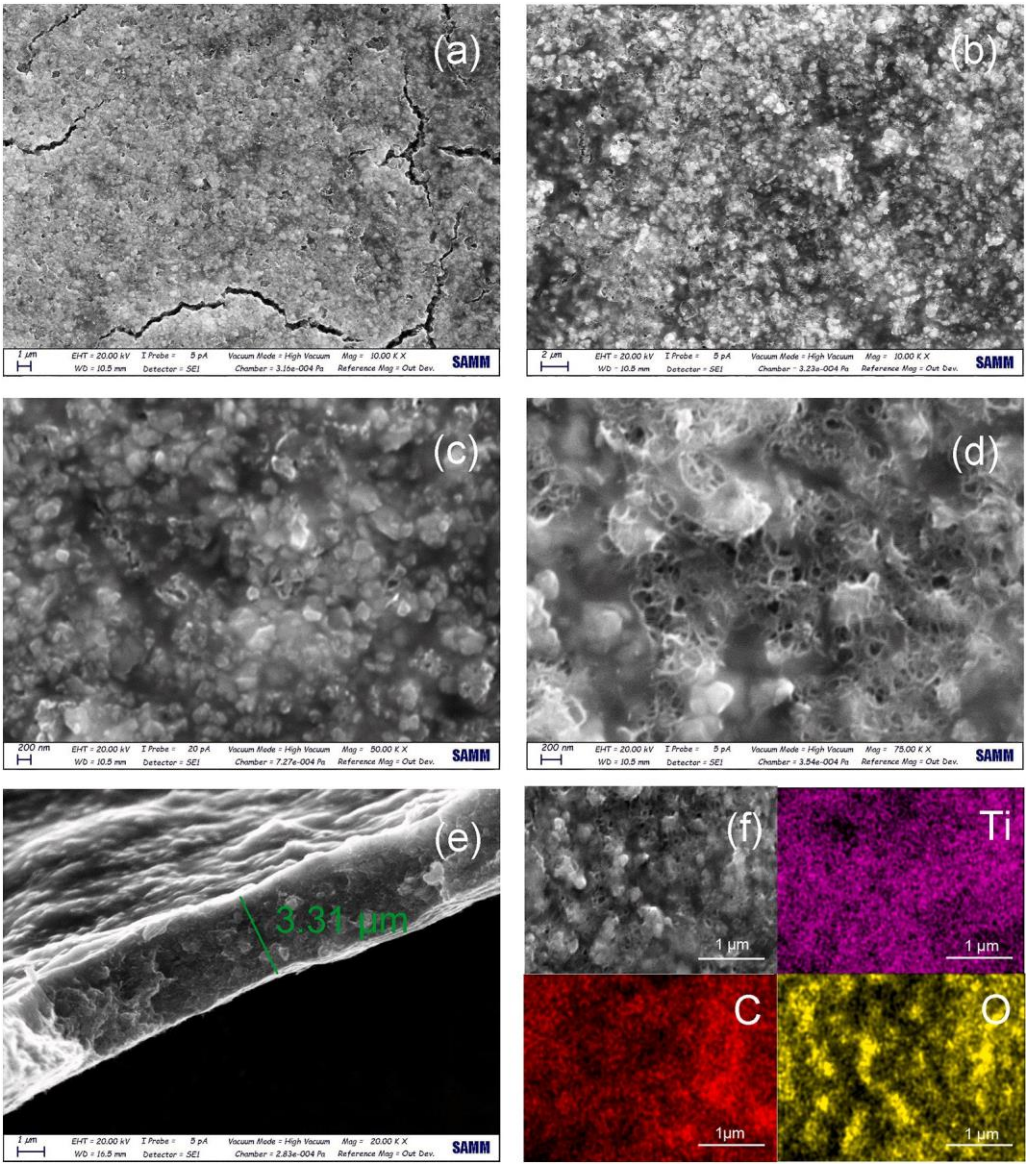

Fig. 2. SEM images at different magnification: LTO-CB electrode top-view at 10 K magnification (a), LTO-CNT electrode top-view at 10 K magnification (b), LTO-CB electrode top-view at 50 K magnification (c), LTO-CNT electrode top-view at 75 K magnification (d), LTO-CNT electrode cross-section at 20 K magnification and corresponding electrode thickness (e). EDS analysis (f) showing the LTO-CNT surface elemental map.

formed in terms of viscosity, surface tension and density in order to collect the inverse of the Ohnesorge number (Oh^{-1}) to define ink printability. The viscosity of the three formulations was measured in order to assess the compatibility with the suitable viscosity range of IJP inks, i.e. 1–25 cP [42]. Fig. 1-a presents the inks viscosity as a function of shear rate and the relative values are reported in Table 1 along with surface tension values. The overall behavior of the three formulations is typical of a Newtonian fluid, i.e. viscosity independent from shear rate. Ink formulation of LTO only, i.e. without conductive agent, had slightly lower viscosity and a coherent trend on viscosity raise was found according to the specific surface area of carbon additive (MWCNT > CB). All inks viscosity values were in the desired range, even at high shear rates and this is favorable as typical shear rates involved during ejection are in the range of 10^4–10^5 s^{-1} [43]. Values of surface tension for three formulations are reported in Table 1. Surface tension values were close to ~40 mN m^{-1}, which is in the appropriate surface tension range of IJP inks, i.e. 25–50 mN m^{-1} [42]. It is well below the water surface tension value (~70 mN m^{-1}) and even lower than commercial black ink (~50 mN m^{-1}), mainly because of the PVP and LDS effect on surface tension lowering. The drop formation behavior in IJP application is typically governed by Oh^{-1} [44], known as Z number, which is determined by ink physical parameters only and is given by Eq. (1):

$$Oh^{-1} = \frac{\sqrt{\sigma * \rho * d}}{\eta} \quad (1)$$

where σ is the ink surface tension, ρ is ink density, d is a characteristic length, usually taken as the nozzle diameter (21 μm), and η is the ink viscosity. Reis and Derby reported $1 < Oh^{-1} < 10$ as a range where printability is optimal [45]. The lower limit represents a condition where viscous forces prevent drop ejection because fluid is too viscous. Moreover, this condition poses serious issues related to nozzle clogging. The upper limit, instead, represents conditions for satellites generation, i.e. smaller droplets separated from the main drop that easily lose directionality [46]: this affects printing quality and precision. As a matter of fact, systems where Oh^{-1} is larger than 10 are still printable with a good final resolution provided that the satellites merge with the head drop at a certain point. Inks with Oh^{-1} values up to 21 were successfully printed [47]. Oh^{-1} values for the formulated inks are reported in Table 1. Being all values close to 10, all formulations were indeed easily printable. It is possible to couple Reynold (Re) number, given in Eq. (2):

$$Re = \frac{v * d * \rho}{\eta} \quad (2)$$

with the Ohnesorge (Oh) number, in order to assess ink printability from a theoretical point of view. The Ohnesorge-Reynold diagram for LTO-CNT ink is reported in Fig. S1. The values for LTO-CB and LTO-no add inks are not reported, as only a small difference passes among them compared to those of LTO-CNT ink. As Re varies with the drop velocity, i.e. the voltage applied to the resistor element, it is possible to select the optimal voltage for the printing process, being V = 11 V, as it corresponds to a drop velocity that is sufficiently high. Z potential value determines stability of nanoparticles suspension in water. Nanoparticles dispersion are stable if Z values are over ±30, when a sufficiently strong electrostatic repulsion among nanoparticles is reached [48]. Values of Z potential for LTO-no add, LTO-CB and LTO-CNT formulations are reported in Table 1. A good stability for all ink formulations was found, confirmed by the absence of evident sediment after several days of storage. Eventually, particle size in the inks is reported in Table 1. Size dimensions are sufficiently small to allow jetting, without nozzle clogging. As a general rule, a clogging-free jetting is forecast when particle size dimension is between $1/100 < d < 1/50$ of the nozzle diameter. Despite LTO-CNT ink having particles dimensions slightly higher than 300 nm (nozzle diameter is 30 μm), no nozzle clogging was observed during printing process. To this extent, CNTs length indeed represents an issue when dealing with inkjet printing, because of nozzle clogging. On the other hand, too short CNTs would not provide the best properties in terms of conductivity. In our formulation we were able to find an optimal compromise that can satisfy both the demands.

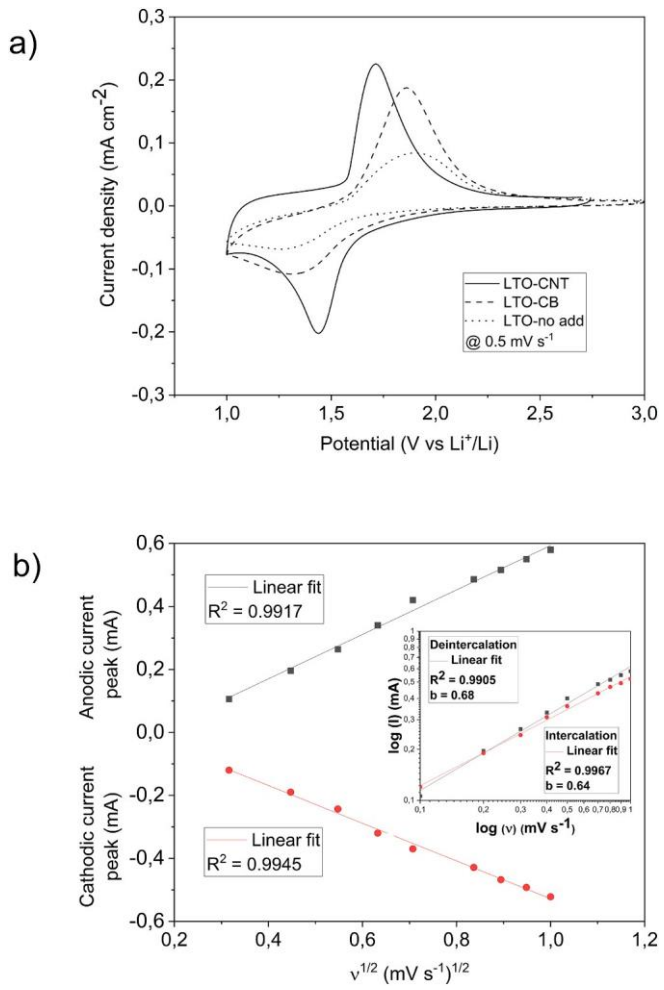

Fig. 3. Comparison of cyclic voltammetry curves at a scan rate of 0.5 mV s^{-1} between LTO-CNT electrode (solid line), LTO-CB electrode (dashed line) and LTO-no add electrode (dotted line) (a) and anodic and cathodic peaks current of LTO-CNT electrode as a function of the square root of the scan rate (b). Inset: plot of the logarithmic value of current peaks as a function of logarithmic value of the scan rate.

4.2. Printed electrode characterization

Images of printed LTO-CNT, LTO-CB and LTO-no add electrodes on Cu plates are reported in Fig. S2. Fig. 2 shows SEM images and compositional map of LTO-CB and LTO-CNT printed electrodes. LTO-CB electrode surface (Fig. 2-a,c) showed a severely cracked surface with cracks distributed all over the surface, suggesting a brittle behavior of the electrode. Fig. S3 shows SEM image and compositional map of the LTO-no add electrode. A similar superficial appearance was found on the LTO-no add electrode, as cracks were present. On the contrary, LTO-CNT printed layer (Fig. 2-b,d) had a less smooth surface but compact and free of cracks. This effect could be attributed to the different morphology of the conductive agent. CB is composed of irregular aggregates of spherical morphology while, on the contrary, CNTs are 1D materials able to create a continuous spider web-like network which contributes to greatly increase the cohesion of the LTO particles, whose dimension was about hundredths of nanometers. Fig. 2-e reports the cross-section of a 20 printed layers-thick LTO-CNT electrode: a uniform thickness of 3.3

Table 2
Diffusion coefficient values for LTO-CNT, LTO-CB and LTO-no add printed electrodes.

	LTO-no add	LTO-CB	LTO-CNT
D_{in} ($*10^{-11}$ cm^2 s^{-1})	0.75	1.73	6.93
D_{de} ($*10^{-11}$ cm^2 s^{-1})	1.10	5.61	8.38

μm was measured, showing a very compact and dense coating that confirms the binding capability of the MWCNT network. From EDS analysis of LTO-CNT electrode (Fig. 2-f), titanium, carbon and oxygen were uniformly distributed, suggesting the absence of any segregation process during the drying of the inkjet-printed layer. The electrical properties of printed electrodes were obtained in terms of sheet resistance (R_s) and resistivity (ρ). The obtained values are reported in Table S2. The results were coherent, as the electrode without a conductive agent had the highest resistivity. As expected, LTO-CNT electrode showed the lowest resistivity compared to the LTO-CB and LTO-no add electrodes. In particular, the MWCNTs decreased the R_s value of an order of magnitude compared to CB, as a good percolative conductive path favored by their aspect ratio was created [49].

4.3. Electrochemical characterization

The electrochemical behavior of various LTO electrodes according to the conductive agent addition was evaluated through cyclic voltammetry (CV). In particular, the LTO/carbon conductive agent ratio is kept to 8:1, in order to effectively extract the active material capacity and do not lower the specific capacity of the battery. CV curves of the three different printed electrodes are presented in Fig. 3-a. Two reversible redox peaks for LTO-CNT electrode were observed, confirming the behavior of LTO nanoparticles with the typical highly reversible reaction Li^+ ions extraction and insertion processes in the LTO spinel structure. The difference between the potentials of the anodic and cathodic current peaks, defined as $\Delta E^{p} = E^{an,p} - E^{cat,p}$, reflected the same trend of sheet resistance, as ΔE^{p} decreased as R_s was lower. The highest values (640 mV) was found for the LTO only, as predictable because of the poor intrinsic electronic conductivity of LTO [50]. Despite an overall enhancement in both ΔE^p and peak current for LTO-CB electrode, only an addition of MWCNTs in the LTO ink was able to give both sharp and well defined anodic and cathodic peaks, suggesting a lower polarization for the charge transfer reaction as results of a much better electrification. Moreover, it is possible to quantify the capacitive (i.e. non-diffusion controlled) and the faradaic diffusion-controlled contributions to the total stored charge. For a battery-like electrode, the peak current is proportional to the square root of the scanning rate, while for a capacitor-like electrode the current dependency on the scan rate is linear [51]. This is summed in Eq. (3)

$$i = Cv^b \tag{3}$$

C and b are adjustable parameters. In particular, b is found as the slope of the plot log I vs log *v* and two conditions can be recognized: b = 0.5 is representative of a battery-like electrode and b = 1 of a capacitor-like electrode [51]. Inset in Fig. 3-b represents the log i vs log ν plot for an LTO-CNT electrode where b was calculated both for the intercalation and deintercalation processes as 0.68 and 0.64, respectively. The capacitive effects related to pseudo-capacitance and double layer charging were not negligible, due to the presence of nano-sized material, according to SEM images. Similarly, b values for the intercalation in LTO-CB and LTO-no add electrodes (Fig. S4-a,b) were 0.59 and 0.52, respectively. This aspect confirms that the storage mechanics is almost purely diffusion controlled as Li^+ intercalation/de-intercalation. In order to understand the nature of the kinetic behavior of the active material, the diffusion coefficient D can be derived by using the Randles-Sevcik Eq. (4) [52]:

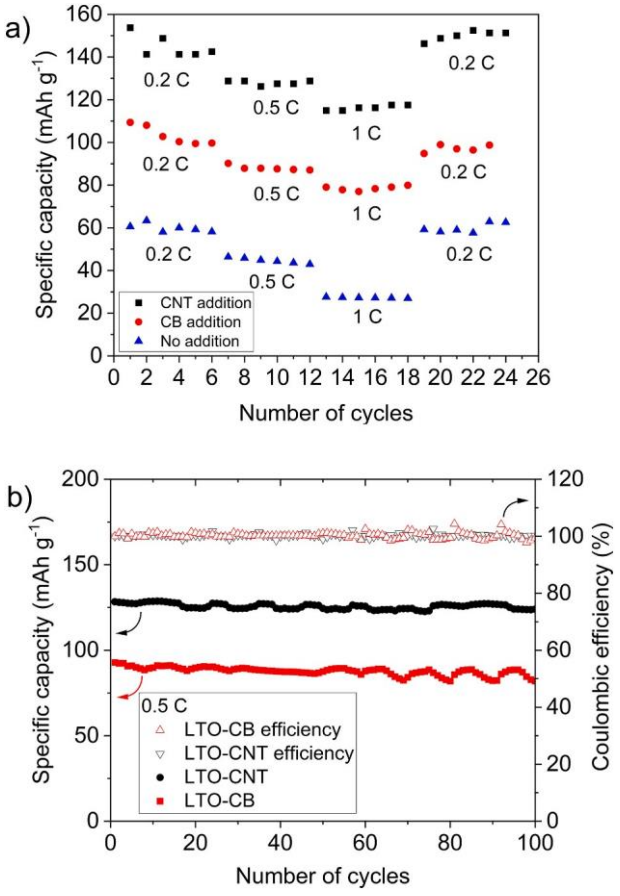

Fig. 4. Comparison of the discharge capacity of three electrodes: LTO-CNT (black), LTO-CB (red) and LTO-no add (blue) vs number of cycles at 0.2 C, 0.5 C and 1 C (a) and discharge capacity and coulombic efficiency on 100 cycles at 0.5 C for LTO-CB electrode and LTO-CNT electrode (b).

$$i_p = 2.69*10^5 A n^{3/2} C^* D^{1/2} v^{1/2} \tag{4}$$

where A is the electrode area, n is the number of electrons involved in redox reaction, C* is the concentration of Li^+ ions in the electrolyte, D is the Li^+ ions diffusion coefficient and ν is the scan rate. The diffusivity of lithium ions is calculated for the intercalation and deintercalation process. The corresponding D values are reported in Table 2 and are in accordance with values found in literature [53,54]. As expected, the LTO-CNT electrode was characterized by a better lithium ions diffusion process compared to LTO-CB and LTO-no add electrodes.

In order to understand the electrochemical performance in terms of storage capacity, galvanic charge-discharge (GCD) curves were obtained at 0.2 C, 0.5 C and 1 C in a voltage window ranging from 1 V to 3 V vs Li^+/Li. Fig. S5 shows the galvanic discharge curves of LTO-no add, LTO-CB and LTO-CNT electrodes. Both LTO-CNT and LTO-CB electrodes showed a visible plateau around 1.53 V. LTO-no add electrode, instead, didn't show a well-defined plateau, resulting in poor capacity value. Fig. 4-a shows the electrodes rate capability. As expected, LTO-CNT electrode showed the best electrochemical performance for every tested C-rate. The specific capacity of LTO-CNT electrode at 0.2 C was 150.3 mAh g^{-1}, which was sensibly higher compared to LTO-CB electrode (101.2 mAh g^{-1}) and LTO-no add electrode (58.9 mAh g^{-1}). After 100 cycles at 0.5 C (Fig. 4-b), LTO-CB capacity faded from 91.3 mAh g^{-1} to 81 mAh g^{-1}. On the other hand, the LTO-CNT electrode showed a higher specific capacity, with an initial value of 128 mAh g^{-1} and almost negligible capacity loss after 100 cycles (Fig. 4-b). In addition, the

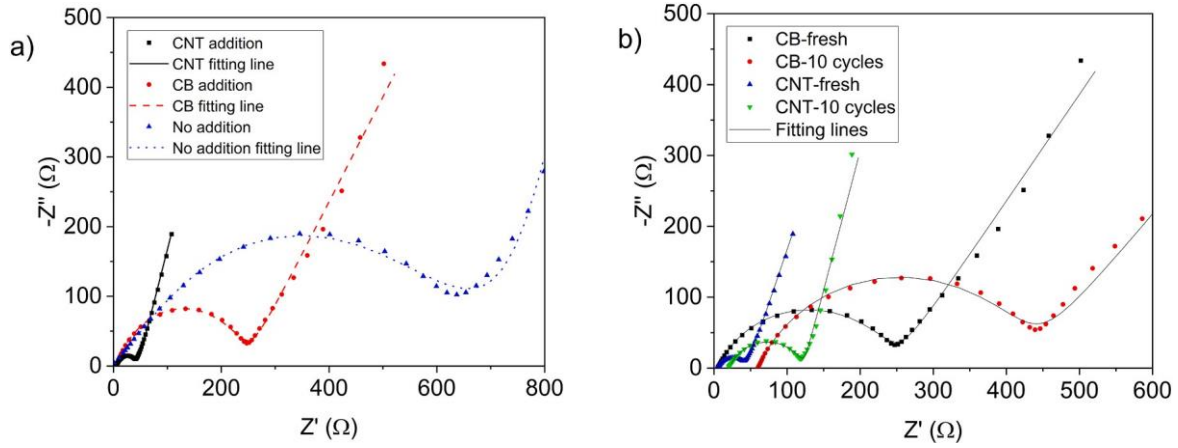

Fig. 5. Nyquist plots of the LTO-CNT (black), LTO-CB (red) and LTO-no add (blue) electrodes (a) and fitting results using an equivalent circuit (inset). Nyquist plot of LTO-CB and for LTO-CNT upon different cycles states (b).

Table 3
Fitted impedance parameters for LTO-no add, LTO-CB and LTO-CNT electrodes.

	No add	CB-fresh	CNT-fresh	CB-10 cycles	CNT-10 cycles
R_2 (Ω)	610.9	240.2	42.33	410.3	101
i^0 (mA cm^{-2})	0.072	0.107	0.611	–	–

average coulombic efficiency was 100%. The results indicate that the addition of CNTs as conductive agent involves a significant improvement in terms of reversible capacity and cycling stability.

The effect of carbon conductive additive on the overall electrochemical properties was further investigated through EIS measurements. The Nyquist plots of LTO-no add, LTO-CB and LTO-CNT electrodes are presented in Fig. 5-a. Fittings were performed using the equivalent circuit represented in the inset in Fig. 5-a. In this equivalent circuit, R_1 represents the electrical contact between the electrode and the graphite current collector resistance and R_2 is the charge transfer resistance. The results obtained from fitting experimental data are reported in Table 3. The corresponding charge transfer resistance for the LTO-CNT electrode was sensibly lower, i.e. 42 Ω, compared to that of LTO-CB and LTO-no add, i.e. 240 Ω and 355 Ω, respectively. It is evident how the addition of a suitable conductive agent improves the charge-transfer reaction, decreasing the overall battery internal impedance. In addition, the exchange current density is calculated according to Eq. (5):

$$i^0 = \frac{RT}{nFR_2} \tag{5}$$

where R is the gas constant, T is the temperature, n is the number of electrons involved, F is the Faraday constant. Corresponding values are listed in Table 3. The exchange current density of LTO-CNT electrode was the highest, compared to those of LTO-CB and LTO-no add, as result of a greater conductivity of CNTs [55]. Fig. 5-b represents the Nyquist plots of LTO-CB and LTO-CNT upon different cycle states. After 10 cycles, charge-transfer resistance increased upon cycling for both LTO-CNT and LTO-CB electrode, as consequence of SEI formation and accumulation on LTO nanoparticles surface. However, the increase was much more restrained for LTO-CNT electrode, likely because of a better electrification given by the continuous MWCNTs network that produced a more homogeneous, stable and thinner SEI compared to the CB loaded electrode.

5. Conclusions

In summary, we have proposed simple aqueous-based $Li_4Ti_5O_{12}$ ink formulations and investigated the effect of carbon conductive additive in terms of ink rheological properties and electrochemical performances of inkjet-printed thin films electrodes. The presence of CNTs contributes to creating a continuous, free of cracks electrode surface, compared to CB-based electrode. Galvanostatic charge-discharge cycles evidenced a specific discharge capacity sensitively higher for electrodes comprising a conductive agent, compared to the one where no carbon addition was done. In particular, a specific discharge capacity for the LTO-CNT electrode of 128 mAh g^{-1} at 0.5 C was observed with no capacity loss after 100 cycles. EIS analysis confirmed that the overall improvement of electrochemical performances is strictly related to the formation of highly electrically conductive percolation path that is dependent on the type of carbon conductive additive. Besides the promising performances for thin-film printed battery applications, the work highlights the importance of a suitable materials choice in ink formulation in order to obtain high-performances thin-film electrodes through inkjet printing.

CRediT authorship contribution statement

Prisca Viviani: Conceptualization, Methodology, Investigation, Data curation, Formal analysis, Writing – original draft, Writing – review & editing. **Eugenio Gibertini:** Conceptualization, Methodology, Investigation, Formal analysis, Writing – review & editing. **Filippo Iervolino:** Methodology, Investigation, Formal analysis. **Marinella Levi:** Supervision, Writing – review & editing. **Luca Magagnin:** Conceptualization, Project administration, Supervision, Writing – review & editing.

Declaration of competing interest

The authors declare that they have no known competing financial interests or personal relationship that could have appeared to influence the work reported in this paper.

References

[1] Nitta N, Wu F, Lee JT, Yushin G. Li-ion battery materials: present and future. Mater. Today 2015;18:252–64. https://doi.org/10.1016/j.mattod.2014.10.040.

[2] Choi K-H, Ahn DB, Lee S-Y. Current status and challenges in printed batteries: toward form factor-free, monolithic integrated power sources. ACS Energy Lett 2018;3:220–36. https://doi.org/10.1021/acsenergylett.7b01086.

[3] Hawley WB, Li J. Electrode manufacturing for lithium-ion batteries—analysis of current and next generation processing. J Energy Storage 2019;25:100862. https://doi.org/10.1016/j.est.2019.100862.

[4] Laurenti M, Garino N, Porro S, Fontana M, Gerbaldi C. Zinc oxide nanostructures by chemical vapour deposition as anodes for Li-ion batteries. J. Alloys Compd. 2015;640:321–6. https://doi.org/10.1016/j.jallcom.2015.03.222.

[5] Xie J, Zhao J, Liu Y, Wang H, Liu C, Wu T, et al. Engineering the surface of LiCoO2 electrodes using atomic layer deposition for stable high-voltage lithium ion batteries. Nano Res. 2017;10:3754–64. https://doi.org/10.1007/s12274-017-1588-1.

[6] Fischer J, Adelhelm C, Bergfeldt T, Chang K, Ziebert C, Leiste H, et al. Development of thin film cathodes for lithium-ion batteries in the material system Li–Mn–O by r. f. magnetron sputtering. Thin Solid Films 2013;528:217–23. https://doi.org/10.1016/j.tsf.2012.08.058.

[7] Kolchanov DS, Mitrofanov I, Kim A, Koshtyal Y, Rumyantsev A, Sergeeva E, et al. Inkjet printing of Li-rich cathode material for thin-film lithium-ion microbatteries. Energ Technol 2020;8:1901086. https://doi.org/10.1002/ente.201901086.

[8] Pang Y, Cao Y, Chu Y, Liu M, Snyder K, MacKenzie D, et al. Additive manufacturing of batteries. Adv. Funct. Mater. 2020;30:1906244. https://doi.org/10.1002/adfm.201906244.

[9] Chang P, Mei H, Zhou S, Dassios KG, Cheng L. 3D printed electrochemical energy storage devices. J. Mater. Chem. A 2019;7:4230–58. https://doi.org/10.1039/C8TA11860D.

[10] L. Hu, H. Wu, F. La Mantia, Y. Yang, Y. Cui, Thin, Flexible secondary Li-ion paper batteries, ACS Nano 4 (2010) 5843–5848. doi: https://doi.org/10.1021/nn1018158.

[11] Sun K, Wei T-S, Ahn BY, Seo JY, Dillon SJ, Lewis JA. 3D printing of Interdigitated Li-ion microbattery architectures. Adv. Mater. 2013;25:4539–43. https://doi.org/10.1002/adma.201301036.

[12] Kang K-Y, Lee Y-G, Shin DO, Kim J-C, Kim KM. Performance improvements of pouch-type flexible thin-film lithium-ion batteries by modifying sequential screen-printing process. Electrochim. Acta 2014;138:294–301. https://doi.org/10.1016/j.electacta.2014.06.105.

[13] Lau G-K, Shrestha M. Ink-jet printing of Micro-electro-mechanical systems (MEMS). Micromachines. 2017;8:194. https://doi.org/10.3390/mi8060194.

[14] Borghetti M, Ghittorelli M, Sardini E, Serpelloni M, Torricelli F. Electrical characterization of PEDOT:PSS strips deposited by inkjet printing on plastic foil for sensor manufacturing. IEEE Trans. Instrum. Meas. 2016;65:2137–44. https://doi.org/10.1109/TIM.2016.2571518.

[15] Chung S, Kim SO, Kwon S-K, Lee C, Hong Y. All-inkjet-printed organic thin-film transistor inverter on flexible plastic substrate. IEEE Electron Device Lett 2011;32:1134–6. https://doi.org/10.1109/LED.2011.2156757.

[16] Yoon B, Ham D-Y, Yarimaga O, An H, Lee CW, Kim J-M. Inkjet printing of conjugated polymer precursors on paper substrates for colorimetric sensing and flexible electrothermochromic display. Adv. Mater. 2011;23:5492–7. https://doi.org/10.1002/adma.201103471.

[17] Hoth CN, Choulis SA, Schilinsky P, Brabec CJ. High photovoltaic performance of inkjet printed polymer:fullerene blends. Adv. Mater. 2007;19:3973–8. https://doi.org/10.1002/adma.200700911.

[18] Chang S-C, Liu J, Bharathan J, Yang Y, Onohara J, Kido J. Multicolor organic light-emitting diodes processed by hybrid inkjet printing. Adv. Mater. 1999;11:734–7. https://doi.org/10.1002/(SICI)1521-4095(199906)11:9<734::AID-ADMA734>3.0.CO;2-D.

[19] Lawes S, Sun Q, Lushington A, Xiao B, Liu Y, Sun X. Inkjet-printed silicon as high performance anodes for Li-ion batteries. Nano Energy 2017;36:313–21. https://doi.org/10.1016/j.nanoen.2017.04.041.

[20] Kang S-H, Kim S, Sohn DK, Ko HS. Analysis of drop-on-demand piezo inkjet performance. Phys. Fluids 2020;32:022007. https://doi.org/10.1063/1.5142023.

[21] O¨zkol E, Ebert J, Uibel K, W¨atjen AM, Telle R. Development of high solid content aqueous 3Y-TZP suspensions for direct inkjet printing using a thermal inkjet printer. J. Eur. Ceram. Soc. 2009;29:403–9. https://doi.org/10.1016/j.jeurceramsoc.2008.06.020.

[22] Li C, Shi H, Ran R, Su C, Shao Z. Thermal inkjet printing of thin-film electrolytes and buffering layers for solid oxide fuel cells with improved performance. Int. J. Hydrog. Energy 2013;38:9310–9. https://doi.org/10.1016/j.ijhydene.2013.05.025.

[23] Calvert P. Inkjet printing for materials and devices. Chem Mater - Chem Mater 2001;13. https://doi.org/10.1021/cm0101632.

[24] Furlani EP. Fluid Mechanics for Inkjet Printing. in: Fundam. Inkjet Print., John Wiley & Sons, Ltd; 2015. p. 13–56. https://doi.org/10.1002/9783527684724.ch2.

[25] Zhao Y, Zhou Q, Liu L, Xu J, Yan M, Jiang Z. A novel and facile route of ink-jet printing to thin film SnO2 anode for rechargeable lithium ion batteries. Electrochim. Acta 2006;51:2639–45. https://doi.org/10.1016/j.electacta.2005.07.050.

[26] Milroy CA, Jang S, Fujimori T, Dodabalapur A, Manthiram A. Inkjet-printed Lithium-sulfur microcathodes for all-printed, integrated nanomanufacturing. Small Weinh. Bergstr Ger 2017;13. https://doi.org/10.1002/smll.201603786.

[27] Zhao Y, Liu G, Liu L, Jiang Z. 500. J. Solid State Electrochem. 2009;13:705–11. https://doi.org/10.1007/s10008-008-0575-6.

[28] Huang J, Yang J, Li W, Cai W, Jiang Z. Electrochemical properties of LiCoO2 thin film electrode prepared by ink-jet printing technique. Thin Solid Films 2008;516:3314–9. https://doi.org/10.1016/j.tsf.2007.09.039.

[29] Delannoy P-E, Riou B, Brousse T, Le Bideau J, Guyomard D, Lestriez B. Ink-jet printed porous composite LiFePO4 electrode from aqueous suspension for microbatteries. J. Power Sources 2015;287:261–8. https://doi.org/10.1016/j.jpowsour.2015.04.067.

[30] Gu Y, Wu A, Sohn H, Mollica C, Iqbal Z, Federici J. Fabrication of rechargeable lithium ion batteries using water-based inkjet printed cathodes. J. Manuf. Process. 2015;20. https://doi.org/10.1016/j.jmapro.2015.08.003.

[31] Huang J-J, Jiang Z-Y. Electrochemical performance of LiMn2O4 thin film electrode fabricated by ink-jet printing technique. Acta Phys. -Chim. Sin. 2008;24:1563–7. https://doi.org/10.3866/PKU.WHXB20080906.

[32] Delannoy P-E, Riou B, Lestriez B, Guyomard D, Brousse T, Le Bideau J. Toward fast and cost-effective ink-jet printing of solid electrolyte for lithium microbatteries. J. Power Sources 2015;274:1085–90. https://doi.org/10.1016/j.jpowsour.2014.10.164.

[33] Das PR, Komsiyska L, Osters O, Wittstock G. PEDOT: PSS as a functional binder for cathodes in Lithium ion batteries. J. Electrochem. Soc. 2015;162:A674. https://doi.org/10.1149/2.0581504jes.

[34] Lee J-H, Wee S-B, Kwon M-S, Kim H-H, Choi J-M, Song MS, et al. Strategic dispersion of carbon black and its application to ink-jet-printed lithium cobalt oxide electrodes for lithium ion batteries. J. Power Sources 2011;196:6449–55. https://doi.org/10.1016/j.jpowsour.2011.03.041.

[35] Hong JK, Lee JH, Oh SM. Effect of carbon additive on electrochemical performance of LiCoO2 composite cathodes. J. Power Sources 2002;111:90–6. https://doi.org/10.1016/S0378-7753(02)00264-1.

[36] Guoping W, Qingtang Z, Zuolong Y, MeiZheng Q. The effect of different kinds of nano-carbon conductive additives in lithium ion batteries on the resistance and electrochemical behavior of the LiCoO2 composite cathodes. Solid State Ionics 2008;179:263–8. https://doi.org/10.1016/j.ssi.2008.01.015.

[37] Huang J, Jiang Z. The preparation and characterization of Li4Ti5O12/carbon nano-tubes for lithium ion battery. Electrochim. Acta 2008;53:7756–9. https://doi.org/10.1016/j.electacta.2008.05.031.

[38] Li X, Qu M, Huai Y, Yu Z. Preparation and electrochemical performance of Li4Ti5O12/carbon/carbon nano-tubes for lithium ion battery. Electrochim. Acta 2010;55:2978–82. https://doi.org/10.1016/j.electacta.2010.01.015.

[39] Xiang H, Tian B, Lian P, Li Z, Wang H. Sol–gel synthesis and electrochemical performance of Li4Ti5O12/graphene composite anode for lithium-ion batteries. J. Alloys Compd. 2011;509:7205–9. https://doi.org/10.1016/j.jallcom.2011.04.065.

[40] Rai AK, Gim J, Kang S-W, Mathew V, Anh LT, Kang J, et al. Improved electrochemical performance of Li4Ti5O12 with a variable amount of graphene as a conductive agent for rechargeable lithium-ion batteries by solvothermal method. Mater. Chem. Phys. 2012;136:1044–51. https://doi.org/10.1016/j.matchemphys.2012.08.048.

[41] He X, Yan B, Zhang X, Liu Z, Bresser D, Wang J, et al. Fluorine-free water-in-ionomer electrolytes for sustainable lithium-ion batteries. Nat. Commun. 2018;9:5320. https://doi.org/10.1038/s41467-018-07331-6.

[42] Tang Z, Fang K, Bukhari MN, Song Y, Zhang K. Effects of viscosity and surface tension of a reactive dye ink on droplet formation. Langmuir. 2020;36:9481–8. https://doi.org/10.1021/acs.langmuir.0c01392.

[43] Wang X, Carr WW, Bucknall DG, Morris JF. High-shear-rate capillary viscometer for inkjet inks. Rev. Sci. Instrum. 2010;81:065106. https://doi.org/10.1063/1.3449478.

[44] Lee A, Sudau K, Ahn KH, Lee SJ, Willenbacher N. Optimization of experimental parameters to suppress nozzle clogging in inkjet printing. Ind. Eng. Chem. Res. 2012;51:13195–204. https://doi.org/10.1021/ie301403g.

[45] Reis N, Derby B. Ink jet deposition of ceramic suspensions: modeling and experiments of droplet formation. MRS Proc. 2000;625:117. https://doi.org/10.1557/PROC-625-117.

[46] Derby B. Inkjet printing of functional and structural materials: fluid property requirements, feature stability, and resolution. Annu. Rev. Mater. Res. 2010;40:395–414. https://doi.org/10.1146/annurev-matsci-070909-104502.

[47] Tekin E, Smith PJ, Schubert US. Inkjet printing as a deposition and patterning tool for polymers and inorganic particles. Soft Matter 2008;4:703–13. https://doi.org/10.1039/B711984D.

[48] Kuznetsova YV, Rempel AA. Size and zeta potential of CdS nanoparticles in stable aqueous solution of EDTA and NaCl 2015;51:5.

[49] Burmistrov I, Gorshkov N, Ilinykh I, Muratov D, Kolesnikov E, Anshin S, et al. Improvement of carbon black based polymer composite electrical conductivity with additions of MWCNT. Compos. Sci. Technol. 2016;129:79–85. https://doi.org/10.1016/j.compscitech.2016.03.032.

[50] Babu B Vikram, Babu K Vijaya, Aregai G Tewodros, Devi L Seeta, Latha B Madhavi, Reddi M Sushma, et al. Structural and electrical properties of Li4Ti5O12 anode material for lithium-ion batteries. Results Phys 2018;9:284–9. https://doi.org/10.1016/j.rinp.2018.02.050.

[51] Liu J, Wang J, Xu C, Jiang H, Li C, Zhang L, et al. Advanced energy storage devices: basic principles, analytical methods, and rational materials design. Adv Sci 2018;5:1700322. https://doi.org/10.1002/advs.201700322.

[52] Mukherjee R, Krishnan R, Lu T-M, Koratkar N. Nanostructured electrodes for high-power lithium ion batteries. Nano Energy 2012;1:518–33. https://doi.org/10.1016/j.nanoen.2012.04.001.

[53] Huynh LTN, Ha CTD, Nguyen VD, Nguyen DQ, Le MLP, Tran V Man. Structure and electrochemical properties of Li4Ti5O12 prepared via low-temperature

precipitation. J. Chemother. 2019;2019:e1727859. https://doi.org/10.1155/2019/1727859.

[54] Yan B, Li M, Li X, Bai Z, Yang J, Xiong D, et al. Novel understanding of carbothermal reduction enhancing electronic and ionic conductivity of $Li_4Ti_5O_{12}$ anode. J. Mater. Chem. A 2015;3:11773–81. https://doi.org/10.1039/C5TA00887E.

[55] Choi Y, Cho S, Lee Y-S. Effect of the addition of carbon black and carbon nanotube to FeS2 cathode on the electrochemical performance of thermal battery. J. Ind. Eng. Chem. 2014;20:3584–9. https://doi.org/10.1016/j.jiec.2013.12.052.

Prisca Viviani received her B.Sc. and M.Sc. in Materials Engineering and Nanotechnology from Politecnico di Milano in 2016 and 2018, respectively. She is currently a PhD candidate in Materials Engineering at Politecnico di Milano under the supervision of Professor Luca Magagnin. Her research interests focus on 3D printing, specifically on inkjet and aerosol printing, for flexible, thin-film electrochemical energy storage devices (lithium-ion batteries) and of polymeric materials for low-E polymeric dampers.

Eugenio Gibertini is currently PhD student at Politecnico di Milano under the guidance of Professor Luca Magagnin. He received his M.Sc. degree in Materials Engineering and Nanotechnology in 2016. His research interest focus on the development of microelectrodes for energy storage applications in textile, Li-ion batteries and nanostructured materials.

Filippo Iervolino is currently a Ph.D. candidate under the supervision of Professor Marinella Levi at the department of Chemistry, Materials and Chemical Engineering of Politecnico di Milano. In the framework of a double degree program, he received his M.Sc. degree in Materials Engineering and Nanotechnology at Politecnico di Milano and his M.A.S. in Mechanical Engineering at Polytechnique Montr`eal in 2019. His research interests are additive manufacturing for electronic applications, with particular interest on inkjet printing and aerosol jet printing, and 3D bioprinting.

Marinella Levi received the M.Sc. degree in chemical engineering and the Ph.D. degree in materials engineering from Politecnico di Milano in 1986 and 1989, respectively. Since 2000, she has been the Coordinator of the Laboratory of Chemistry and Characterization of Innovative Polymers. In 2013, she founded +LAB, the first 3D printing laboratory at Politecnico di Milano. She is currently a Full Professor of Material Science and Technology with the Department of Chemistry, Material and Chemical Engineering, Politecnico di Milano. Her current research topics are about design, synthesis and characterization of advanced polymers and composites for additive manufacturing, electronics, and sustainable materials. She has coauthored 160 referred papers and 7 monographies.

Luca Magagnin received the M.Sc. degree in nuclear engineering and the Ph.D. degree in electrochemical engineering from Politecnico di Milano, Milan, Italy. He is currently a Full Professor of Surface Engineering and Materials for Electronics with Politecnico di Milano. He has authored or coauthored more than 100 publications (papers, patents, and book chapters). His main research areas include electrodeposition and electroless plating, surface science and engineering, corrosion, MEMS and development, fabrication and testing of innovative functional materials and coatings.